



CHALMERS

Chalmers Publication Library

Mesoscale modelling of crack-induced diffusivity in concrete

This document has been downloaded from Chalmers Publication Library (CPL). It is the author's version of a work that was accepted for publication in:

Computational Mechanics (ISSN: 0178-7675)

Citation for the published paper:

Nilenius, F. ; Larsson, F. ; Lundgren, K. et al. (2015) "Mesoscale modelling of crack-induced diffusivity in concrete". *Computational Mechanics*, vol. 55(2), pp. 359-370.

<http://dx.doi.org/10.1007/s00466-014-1105-2>

Downloaded from: <http://publications.lib.chalmers.se/publication/210361>

Notice: Changes introduced as a result of publishing processes such as copy-editing and formatting may not be reflected in this document. For a definitive version of this work, please refer to the published source. Please note that access to the published version might require a subscription.

Chalmers Publication Library (CPL) offers the possibility of retrieving research publications produced at Chalmers University of Technology. It covers all types of publications: articles, dissertations, licentiate theses, masters theses, conference papers, reports etc. Since 2006 it is the official tool for Chalmers official publication statistics. To ensure that Chalmers research results are disseminated as widely as possible, an Open Access Policy has been adopted. The CPL service is administrated and maintained by Chalmers Library.

(article starts on next page)

Computational homogenization of crack-induced diffusivity in concrete

Filip Nilenius^{1,2}, Fredrik Larsson², Karin Lundgren¹, and
Kenneth Runesson²

¹ *Department of Civil and Environmental Engineering*

² *Department of Applied Mechanics,*

Chalmers University of Technology, Göteborg, Sweden

Abstract

Cracks have large impact on the diffusivity of concrete since they provide low-resistance pathways for moisture and chloride ions to migrate through the material. In this work, crack-induced diffusivity in concrete is modelled and computationally homogenized on the mesoscale. Computations are carried out on three-dimensional Statistical Volume Elements (SVEs) comprising the mesoscale constituents in terms of cement paste, aggregates and the Interfacial Transition Zone (ITZ). The SVEs are subjected to uni-axial tension loading and cracks are simulated by use of an isotropic damage model. Increased diffusivity is then assigned to the damaged finite elements in the SVE.

In a damaged finite element, the crack plane is assumed to be perpendicular to the largest eigenstrain, and diffusivity is increased only in the in-plane direction of the crack by anisotropic constitutive modelling. Since the developed global crack in the SVE will be non-planar because of the presence of aggregates, the crack-induced homogenized diffusivity of the SVE becomes by this procedure intrinsically anisotropic.

Numerical results show that the macroscale diffusivity of concrete can be correlated to the applied mechanical straining of the SVE and that the macroscale diffusivity increases mainly in the transversal direction relative to the axis of imposed mechanical straining.

Acronyms

3D:	three-dimensional
CH:	computational homogenization
FE:	finite element
ITZ:	Interfacial Transition Zone
SVE:	Statistical Volume Element

Nomenclature

Subscripts

a	aggregate
cp	cement paste
cr	crack
d	damage
el	elastic
ITZ	Interfacial Transition Zone
l	loading
P	planar direction
tang	tangent
I	largest eigenvalue
T	transversal direction
ul	unloading
D	part of boundary with Dirichlet boundary conditions
N	part of boundary with Neumann boundary conditions
p	prescribed

Greek letters

Γ_{\square}	boundary of SVE domain
κ	largest equivalent strain
ω	damage parameter
Ω_{\square}	SVE domain
ε	strain tensor

σ stress tensor

Roman lower case letters

\bar{x}	centroid of SVE
t_{ITZ}	thickness of ITZ
u	displacement
t	time
h	element size
n_a	volume fraction of aggregates
w	width

Misc.

$[\bullet]$	matrix representation in Voigt notation
\square	SVE

Superscripts

M	macroscale
s	subscale

Roman capital letters

\bar{D}	macroscale diffusivity tensor
D_{\bullet}	diffusivity coefficient
D_{\bullet}	diffusivity tensor
J	flux vector
E	stiffness tensor
E_{tang}	algorithmic tangent stiffness tensor
$E_{d,l}$	damaged stiffness tensor during loading
$E_{d,ul}$	damaged stiffness tensor during unloading
n	normal vector
E	Young's modulus
G	shear modulus
L_{\square}	side length of SVE
V	volume

1 Introduction

The diffusivity of concrete is of importance for the service life of most concrete structures, since the diffusivity enables chloride ions to penetrate through the material and initiate reinforcement corrosion. The magnitude of the diffusivity is governed by many factors both in terms of shrinkage, micro-cracking, age and degradation, as well as the mechanical loading history of the material. This complexity makes material modelling challenging if many of these factors are to be considered concurrently.

Cracks¹ in the cement paste will substantially increase the chloride ingress rate and subsequently lead to premature reinforcement corrosion. Therefore, the diffusivity of concrete attributed to cracking has been under extensive study and modelling for a long time by several authors: Gérard et al. [4] developed an early technique to experimentally correlate crack width with permeability, whereas Gérard and Marchand [3] proposed a simple model to predict the effect of cracking on diffusivity by the use of two parameters: crack density and mean crack aperture. Jang et al. [8] carried out experiments which suggested a linear relationship between crack width and diffusivity, and Liu et al. [11] modelled increased diffusivity due to cracking using 3D diffusive lattice networks for problems of both tensile loading and frost. In the work of Grassl [5], the author proposes a model which coupled flow in cracked concrete by means of a damage-plasticity model in conjunction with lattice elements.

However, crack-induced diffusivity in concrete within a computational homogenization context has, to the authors' knowledge, not yet been reported in the literature. Computational homogenization as a technique to determine homogenized material properties has great potential within this field, since it provides a rigorous theoretical framework which can be utilized numerically to correlate subscale crack patterns to macroscale diffusivity while accounting for the heterogeneous mesoscale structure of the material. Using computational homogenization to derive macroscale diffusivity of concrete influenced by material cracking on the mesoscale is the objective of this work.

In this paper, we model concrete on the mesoscale as a heterogeneous three phase and three-dimensional (3D) material, contained within a Statistical Volume Element (SVE). By imposing uni-axial tension loading in a preprocessing step, cracks are computed using an isotropic damage model and the cracks are assigned anisotropic diffusivity properties based on the orientation of the cracks, cf. Algorithm 1 below.

¹we macro-cracks, as opposed to micro-cracks.

Algorithm 1 Computational algorithm to obtain macroscale diffusivity.

- 1: Generate the SVE based on given sieve curve and volume fraction of aggregates, cf. Algorithm 2.
 - 2: Subject SVE to uni-axial deformation and compute crack widths in damaged finite elements in each deformation step.
 - 3: Assign constitutive model of diffusivity for cracked elements according to Eq. (12).
 - 4: **for** selected load steps **do**
 - 5: Solve the stationary boundary value problem of mass transport based on macroscale Dirichlet boundary conditions.
 - 6: Homogenize mass flow obtained from the previous step to yield homogenized macroscale diffusivity.
 - 7: **end for**
-

2 Mesoscale model

We will employ a heterogeneous three-dimensional (3D) mesoscale model of concrete developed in a previous work by the authors, see Nilenius et al. [14] for a detailed description. The model constitutes concrete as a three-phase composite material consisting of cement paste, aggregates and the Interfacial Transition Zone (ITZ), cf. Figure 1. The aggregates are modelled as spheres and can be of arbitrary size and quantity, while the ITZ is an interface material between the cement paste and aggregates characterized by high diffusivity and low stiffness. The mesoscale model is contained within a Statistical Volume Element (SVE) which is generated according to Algorithm 2.

Algorithm 2 Algorithm to generate SVE

- 1: **while** the volume fraction of aggregates inside the SVE is smaller than desired **do**
 - 2: Generate aggregate from given sieve curve.
 - 3: Place the new aggregate at a random point in the SVE.
 - 4: **if** new particle overlaps already existing particle **then**
 - 5: Remove the new aggregate.
 - 6: **else**
 - 7: Add volume of the new aggregate to the accumulated aggregate volume.
 - 8: **end if**
 - 9: **end while**
-

2.1 Finite element discretization

The finite element (FE) discretization is carried out by subdividing the SVE into a structured grid of equally sized voxels which make up 8-node solid finite elements, cf. Figure 1. This discretization approach for 3D domains has also been employed by

Garboczi [2] and Hain and Wriggers [6, 7] for heterogeneous modelling of cement paste and concrete, respectively.

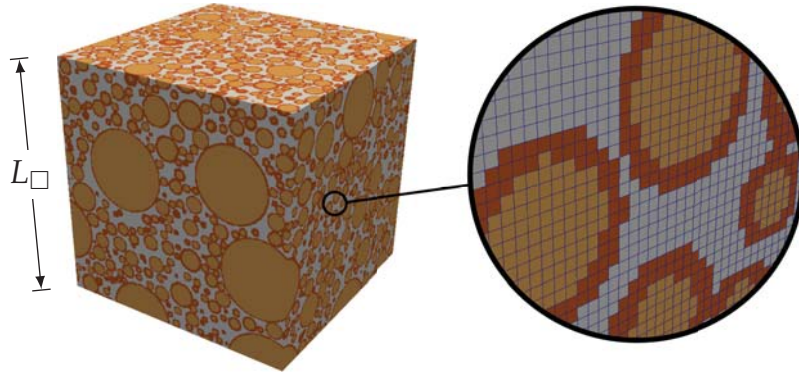


Figure 1: Example of an FE-discretized SVE. The brown-red elements contain ITZ and are described in detail in Section 2.3. The blue-gray elements and yellow-brown elements contain cement paste and aggregates, respectively.

2.2 Constitutive relations for the mesoscale materials

For material diffusivity, we will use a constitutive relation for the mesoscale constituents on the form

$$J = -D \cdot \nabla \phi, \quad (1)$$

where J is the mass flux [$\text{g}/(\text{cm}^2 \text{s})$], D is the second order diffusivity tensor [cm^2/s], ∇ is the spatial gradient operator [$1/\text{cm}$] and ϕ is mass concentration [g/cm^3]. The diffusivity tensors are given for each material² as

$$D_{\text{cp}} = D_{\text{cp}} I, \quad D_{\text{a}} = D_{\text{a}} I, \quad (2)$$

where I is the unit tensor and D_{\bullet} are diffusion coefficients. The expressions for the diffusivity tensors for the ITZ and cracked cement paste are given in Section 2.3 and Section 2.4, respectively. Constitutive relations pertaining to the mechanical problem are discussed in Section 3.1.

2.3 ITZ implementation

The effects of ITZ on the material properties of concrete are implemented for both diffusion and mechanical considerations. When the SVE is discretised into a structured grid, a number of finite elements will contain all three mesoscale constituents of cement paste, aggregates and ITZ, cf. Figure 2. The material properties of these elements are explained in the following two subsections.

²a = aggregate, cp = cement paste.

A variety of strategies to account for the effects of the ITZ have been devised in the literature: Wang and Ueda [18] used lattice elements to model the effects of ITZ, whereas Kim and Al-rub [9] chose to fully resolve the ITZ in the FE-mesh. In this work, the effects of the ITZ will be included using analytical rules of mixtures of Voigt and Reuss type. In this way, the material properties of the elements containing all three mesoscale constituents will be averaged to yield effective properties and no additional elements are needed for this choice of ITZ implementation.

Several authors have shown the ITZ to have a significant influence on the material properties of concrete, cf. Nilsen and Monteiro [15] and Simeonov and Ahmad [17]. Consequently, to account for the ITZ is important regardless of the modelling approach preferred.

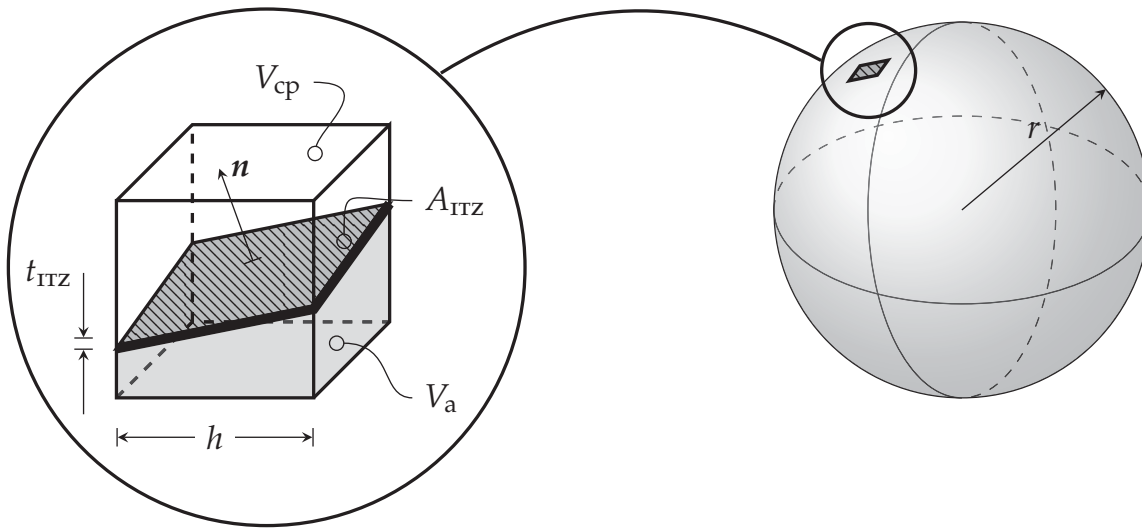


Figure 2: Voxel (left) including the ITZ interface located on the surface of a spherical aggregate (right). The interface voxels contain all three mesoscale constituents and analytical rules of mixture are employed to model overall element properties. The element properties will depend on the normal of the ITZ surface, \mathbf{n} .

2.3.1 Diffusivity

The diffusivity tensor of the interface elements is computed via direct averaging using a Voigt assumption on the form

$$\mathbf{D}_{\text{ITZ}} = \frac{V_a D_a + V_{\text{cp}} D_{\text{cp}}}{h^3} \mathbf{I} + \frac{A_{\text{ITZ}} D_{\text{ITZ}} t_{\text{ITZ}}}{h^3} (\mathbf{I} - \mathbf{n} \otimes \mathbf{n}), \quad (3)$$

where D_{\bullet} are diffusivity coefficients, V_{\bullet} are volumes [cm^3] of aggregate and cement paste, \mathbf{n} and A_{ITZ} is the normal and area [cm^2], respectively, of the ITZ as shown in Figure 2. Generally, we have that $D_a \ll D_{\text{cp}} \ll D_{\text{ITZ}}$. The unknown parameters in Eq. (3) include the thickness, t_{ITZ} , and the diffusivity of the ITZ, D_{ITZ} . Computationally, the

product of these two, $D_{\text{ITZ}} \times t_{\text{ITZ}}$ in units of cm^3/s , becomes the model parameter and the auxiliary notation

$$\hat{D}_{\text{ITZ}} \stackrel{\text{def}}{=} D_{\text{ITZ}} \times t_{\text{ITZ}}, \quad (4)$$

$$\hat{D}_{\text{cp}} \stackrel{\text{def}}{=} D_{\text{cp}} \times 1 \text{ cm}, \quad (5)$$

will be used for the numerical examples in Section 5.

2.3.2 Elasticity

The elastic properties of the ITZ are modelled to be transversally isotropic, where the surface of the ITZ constitutes the plane of isotropy. A local coordinate system is introduced in the interface elements, cf. Figure 3, where the transversal direction, denoted τ , is parallel to the normal of the ITZ surface and the plane of isotropy, denoted ρ , is spanned by the two axes x' and y' that constitute the ITZ surface.

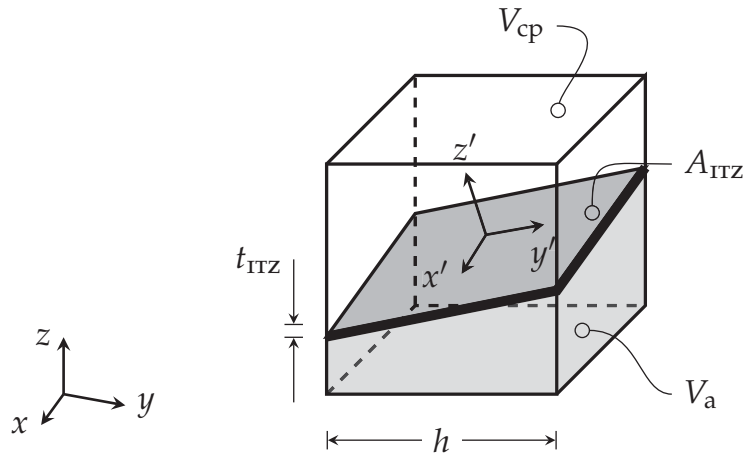


Figure 3: Global coordinate system (left) and local coordinate system in an element located in the ITZ plane. The plane of isotropy is spanned by the two axes x' and y' , whereas the transversal direction is z' .

In the local coordinate system, the strain-stress relation in Voigt notation is given on matrix form as

$$[\varepsilon'] = [\mathbf{S}'][\sigma'], \quad (6)$$

where superscript prime denotes the local coordinate system and $[\bullet]$ denotes matrix representation in Voigt notation. Eq. (6) takes the explicit form

$$\begin{aligned}
\underbrace{\begin{bmatrix} \varepsilon_{x'x'} \\ \varepsilon_{y'y'} \\ \varepsilon_{z'z'} \\ \varepsilon_{y'z'} \\ \varepsilon_{z'x'} \\ \varepsilon_{x'y'} \end{bmatrix}}_{[\varepsilon']} &= \underbrace{\begin{bmatrix} \frac{1}{E_P} & -\frac{\nu_P}{E_P} & -\frac{\nu_{TP}}{E_T} & 0 & 0 & 0 \\ -\frac{\nu_P}{E_P} & \frac{1}{E_P} & -\frac{\nu_{TP}}{E_T} & 0 & 0 & 0 \\ -\frac{\nu_{PT}}{E_P} & -\frac{\nu_{PT}}{E_P} & \frac{1}{E_T} & 0 & 0 & 0 \\ 0 & 0 & 0 & \frac{1}{G_{PT}} & 0 & 0 \\ 0 & 0 & 0 & 0 & \frac{1}{G_{PT}} & 0 \\ 0 & 0 & 0 & 0 & 0 & \frac{2(1+\nu_P)}{E_P} \end{bmatrix}}_{[\mathbf{S}']} \underbrace{\begin{bmatrix} \sigma_{x'x'} \\ \sigma_{y'y'} \\ \sigma_{z'z'} \\ \sigma_{y'z'} \\ \sigma_{z'x'} \\ \sigma_{x'y'} \end{bmatrix}}_{[\sigma']} \quad (7)
\end{aligned}$$

where E_\bullet , G_\bullet and ν are Young's modulus, shear modulus and Poisson's ratio, respectively. Mapping of the compliance matrix $[\mathbf{S}']$ from the local to the global coordinate system is conducted via the transformation matrix $[A_\varepsilon]$ according to the expression

$$[\mathbf{S}] = [A_\varepsilon]^T [\mathbf{S}'] [A_\varepsilon], \quad (8)$$

where $[A_\varepsilon] = [A_\varepsilon](\mathbf{n})$ is the transformation matrix which is dependent on the surface normal of the ITZ, \mathbf{n} .

The in-plane Young's modulus, E_P , is computed using Voigt's rule of mixture

$$E_P = \frac{1}{h^3} (V_a E_a + V_{cp} E_{cp} + A_{ITZ} t_{ITZ} E_{ITZ}). \quad (9)$$

and Young's modulus in the transversal direction, E_T , is computed by the use of Reuss' rule of mixture

$$\frac{h^3}{E_T} = \frac{V_a}{E_a} + \frac{V_{cp}}{E_{cp}} + \frac{A_{ITZ} t_{ITZ}}{E_{ITZ}}, \quad (10)$$

where h is the element size, cf. Figure 2, and E_{ITZ} is the Young's modulus of ITZ which is assumed to be a scaled value of E_{cp} on the form

$$E_{ITZ} = \alpha E_{cp}, \quad \text{where } \alpha \in (0, 1). \quad (11)$$

By Eq. (10), E_T will approximately equal E_{ITZ} for a sufficiently large A_{ITZ} . The motivation for this formulation is that the ITZ constitutes a weak zone in concrete through which cracks tend to propagate. The stiffness in the transversal direction should, therefore, be governed by the stiffness of the ITZ to capture this effect. Furthermore, the

elastic strain will tend to concentrate in the ITZ, initiating the development of cracks. However, since the third term on the right hand side of Eq. (9) will be much smaller in magnitude than the other two, the stiffness will in the plane of isotropy be governed by the stiffness of cement paste and aggregate. Effectively, the ITZ will only influence, i.e. reduce, the element stiffness in the transverse direction.

Experimental data for E_{ITZ} are scarce in the literature. For the numerical examples in Section 5 based on experimental data from Barbosa and Carneiro [1], we will use $\alpha = 0.45$ in Eq. (11).

Remark. *The ITZ implementation adopted here pertains to the case of concrete subjected to tension loading. In the case of imposed compression, a different ITZ model would have to be considered.*

2.4 Crack-induced diffusivity

The increased diffusivity attributed to cracking is modelled in the same fashion as the diffusivity of ITZ described in Section 2.3.1. The crack plane in a damaged element is assumed to be perpendicular to the eigenvector, \mathbf{n}_I , associated with the largest principal strain, cf. Figure 4. The element diffusivity is then expressed as

$$\mathbf{D}_{cr} = \mathbf{D}_{cp} + \frac{A_{cr} D_{cr} w_{cr}}{h^3} (\mathbf{I} - \mathbf{n}_I \otimes \mathbf{n}_I), \quad (12)$$

where w_{cr} is the crack width, A_{cr} the crack area and D_{cr} the diffusivity of the crack, cf. Figure 4. The crack width w_{cr} can be computed as

$$w_{cr} = h \mathbf{n}_I \cdot \left[\boldsymbol{\varepsilon} - \underbrace{\mathbf{E}^{-1} : \boldsymbol{\sigma}}_{\boldsymbol{\varepsilon}_{el} = (1-\omega)\boldsymbol{\varepsilon}} \right] \cdot \mathbf{n}_I = h \omega \varepsilon_I. \quad (13)$$

where the damage parameter ω is defined in the following section.

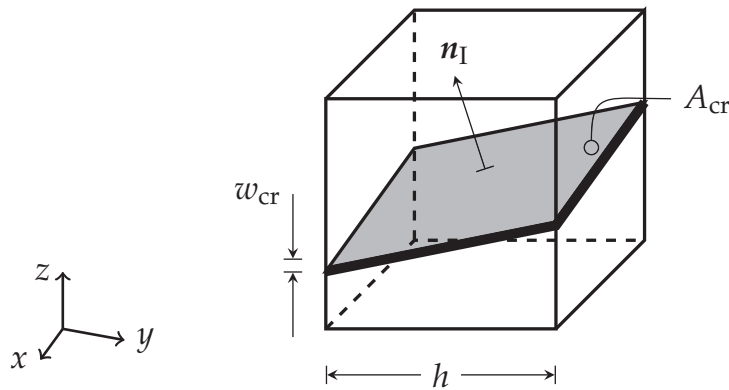


Figure 4: *Damaged element with a crack plane perpendicular to \mathbf{n}_I with an associated crack area A_{cr} . The crack plane is assumed to be perpendicular to the largest principal strain direction, \mathbf{n}_I .*

3 Stress analysis

3.1 Damage model

The modelling of damage is not the main objective of this paper; it will merely serve as a preprocessor tool to determine possible crack patterns in the cement paste in which diffusivity will be increased. Furthermore, for the numerical example, we will only consider the case of uni-axial tension. Hence, we will only model damage due to tension and not compression.

The damage model will be used as a smeared crack model. An isotropic damage model for the cement paste and interface voxels/elements³ will be employed on the form

$$\boldsymbol{\sigma} = (1 - \omega)\mathbf{E} : \boldsymbol{\varepsilon}, \quad (14)$$

where $\omega = \omega(\kappa)$ is a scalar damage parameter, cf. Figure 5, given by the relation (Mazars [12])

$$\omega(\kappa) = \begin{cases} 0 & \text{if } \kappa \leq \varepsilon_{\text{cr}}, \\ 1 - (1 - A)\frac{\varepsilon_{\text{cr}}}{\kappa} - A \exp[-B(\kappa - \varepsilon_{\text{cr}})] & \text{if } \kappa \geq \varepsilon_{\text{cr}}. \end{cases} \quad (15)$$

In Eq. (15), A and B are model parameters, ε_{cr} the strain at which cracking is initiated and κ , in turn, a measurement of the largest equivalent strain, $\tilde{\varepsilon}$, ever reached in the loading history of the material, expressed as

$$\kappa(t) = \max_{\tau \leq t} \tilde{\varepsilon}(\tau), \quad (16)$$

where t denotes time. The equivalent strain is expressed in energy norm as

$$\tilde{\varepsilon} = \sqrt{\frac{\langle \boldsymbol{\varepsilon} \rangle : \mathbf{E} : \langle \boldsymbol{\varepsilon} \rangle}{E}}, \quad \langle \boldsymbol{\varepsilon} \rangle \stackrel{\text{def}}{=} \sum_{I=1}^3 \langle \varepsilon_I \rangle \mathbf{n}_I \otimes \mathbf{n}_I, \quad (17)$$

and $\langle \bullet \rangle$ denotes Macaulay brackets, i.e. $\langle x \rangle = \max(0, x)$ for scalars.

³since aggregate elements are modelled without damage, they remain elastic.

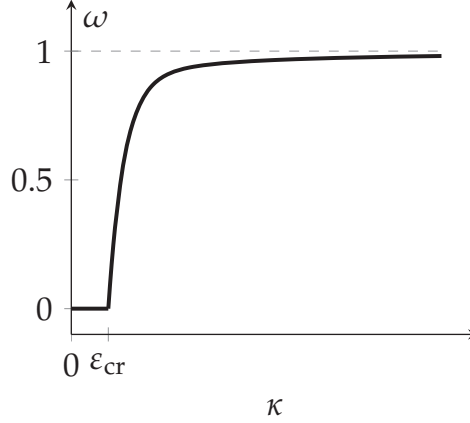


Figure 5: Eq. (15) graphed for $A = 0.81$, $B = 10,450$, and $\varepsilon_{\text{cr}} = 1 \times 10^{-4}$ (parameter values suggested by Saouridis [16]). The damage parameter ω increases rapidly in value once $\kappa > \varepsilon_{\text{cr}}$ and then asymptotically approaches full damage at $\omega = 1$.

3.2 Boundary conditions on SVE

We will impose boundary conditions on the SVE on the form

$$\mathbf{u} = \bar{\mathbf{u}} + \bar{\boldsymbol{\varepsilon}} \cdot [\mathbf{x} - \bar{\mathbf{x}}] \quad \forall \mathbf{x} \in \Gamma_{\square,z} \subset \Gamma_{\square}, \quad (18)$$

where $\bar{\mathbf{x}}$ denotes the center coordinate of the SVE, $\bar{\mathbf{u}}$ the macroscale displacement and $\bar{\boldsymbol{\varepsilon}}$ the macroscale strain tensor expressed on the form

$$[\bar{\boldsymbol{\varepsilon}}] = \begin{bmatrix} -\bar{\nu} & 0 & 0 \\ 0 & -\bar{\nu} & 0 \\ 0 & 0 & 1 \end{bmatrix} \bar{\varepsilon}_{zz}, \quad (19)$$

where $\bar{\varepsilon}_{zz}$ is the prescribed normal strain evolution in the z -direction. Here, $\Gamma_{\square,z}$ denotes that part of the boundary where normal is in either positive or negative z -direction. The remaining part of the boundary is said to be traction free. The structure of $\bar{\boldsymbol{\varepsilon}}$ in Eq. (19) represents an approximation of uni-axial tension in the z direction. By this choice of boundary conditions, it will be possible to computationally correlate macroscale strain increments to macroscale diffusivity.

The part of the boundary conditions describing the Poisson effect in the lateral directions, $-\bar{\nu}\bar{\varepsilon}_{zz}$, is only accurate for an SVE of homogeneous material. For an SVE of heterogeneous materials—as considered in this work—the Poisson effect is only approximate because the SVE boundaries will not contract uniformly.

4 Macroscale diffusivity

We wish to establish a macroscopic constitutive relation on the form

$$\bar{\mathbf{J}} = -\bar{\mathbf{D}} \cdot \bar{\nabla} \bar{\phi}, \quad (20)$$

where $\bar{\bullet}$ denotes a macroscopic quantity, \bar{J} the macroscale flux, \bar{D} the macroscale diffusivity tensor and $\bar{\nabla}\bar{\phi}$ the macroscale gradient of some macroscale potential $\bar{\phi}$. In particular, the dependence of the macroscopic diffusivity tensor on macroscale strain increments will be determined.

The homogenization procedure stems from the fully resolved, stationary, boundary value problem of determining the potential $\phi(x)$ from the balance equation

$$\nabla \cdot J = 0 \quad \forall x \in \Omega, \quad (21)$$

for which all material heterogeneities are embedded in $\Omega \subset \mathbb{R}^3$. Here, ∇ is the nabla operator and $J(x)$ the flux of some generic physical quantity. We consider the linear constitutive relation

$$J = -D \cdot \nabla \phi, \quad (22)$$

where D varies in space as discussed in Section 2. By e.g. adopting variationally consistent homogenization, as proposed by Larsson et al. [10], the macroscale flux can be established as

$$\bar{J} = \langle J \rangle_{\square}, \quad (23)$$

where $\langle \bullet \rangle_{\square}$ denotes the volume average

$$\langle \bullet \rangle_{\square} \stackrel{\text{def}}{=} \frac{1}{|\Omega_{\square}|} \int_{\Omega_{\square}} \bullet \, d\Omega_{\square}, \quad (24)$$

The considered SVE Ω_{\square} is centered at the macroscale position $\bar{x} \in \Omega$; hence, $\langle x - \bar{x} \rangle_{\square} = 0$.

Assuming separation of scales, we consider a unique SVE at each macroscale coordinate x . It is then possible to introduce the split of a scalar field ϕ within Ω_{\square} into the macroscale and fluctuation parts⁴ as follows:

$$\phi(x; \bar{x}) = \phi^M(x; \bar{x}) + \phi^s(x). \quad (25)$$

Adopting first order homogenization, the macroscale part is assumed to vary linearly

$$\phi^M(x; \bar{x}) = \bar{\phi}(\bar{x}) + \bar{g}(\bar{x}) \cdot [x - \bar{x}] \quad \forall x \in \Omega_{\square}, \quad (26)$$

with $\bar{g} \stackrel{\text{def}}{=} \bar{\nabla}\bar{\phi}$. Hence, we obtain $\nabla\phi^M(\bar{x}; \bar{x}) = \bar{g}(\bar{x})$ constant within Ω_{\square} .

Adopting Dirichlet boundary conditions, the local fluctuations $\phi^s \in \boldsymbol{\phi}^s = \{\phi \text{ sufficiently regular, } \phi = 0 \text{ on } \Gamma_{\square}\}$ can be solved from

$$\frac{1}{|\Omega_{\square}|} \int_{\Omega_{\square}} \nabla\delta\phi^s \cdot D \cdot (\bar{g} + \nabla\phi^s) \, d\Omega = 0 \quad \forall \delta\phi^s \in \boldsymbol{\phi}^s. \quad (27)$$

As a result, the homogenized flux can be computed as the implicit relation

$$\bar{J} = \bar{J}\{\bar{g}\} = -\langle D \cdot (\bar{g} + \nabla\phi^s) \rangle_{\square}. \quad (28)$$

⁴Superscripts M and s denote macroscale and subscale, respectively.

In order to establish the macroscale tensor $\bar{\mathbf{D}}$ expressed in Eq. (20), the linearity of Eqs. (27) and (28) can be utilized. Following Nilenius et al. [14], we can express the subscale fluctuation as

$$d\phi^s = \sum_{i=1}^3 \hat{\phi}_{\bar{\mathbf{g}}}^{s(i)} \mathbf{e}_i \cdot d\bar{\mathbf{g}}, \quad (29)$$

where \mathbf{e}_i are the orthonormal basis vectors. The unit fields $\hat{\phi}_{\bar{\mathbf{g}}}^{s(i)} \in \boldsymbol{\phi}^s$ can be solved from

$$\frac{1}{|\Omega_{\square}|} \int_{\Omega_{\square}} \nabla \delta\phi^s \cdot \mathbf{D} \cdot \nabla \hat{\phi}_{\bar{\mathbf{g}}}^{s(i)} d\Omega = -\frac{1}{|\Omega_{\square}|} \int_{\Omega_{\square}} \nabla \delta\phi^s \cdot \mathbf{D} \cdot \mathbf{e}_i d\Omega \quad \forall \delta\phi^s \in \boldsymbol{\phi}^s, \quad (30)$$

for $i = 1, 2, 3$. Based on the unit fields, the effective diffusivity becomes

$$\bar{\mathbf{D}} = \langle \mathbf{D} \rangle_{\square} + \sum_{i=1}^3 \left\langle \mathbf{D} \cdot \nabla \hat{\phi}_{\bar{\mathbf{g}}}^{s(i)} \right\rangle_{\square} \otimes \mathbf{e}_i. \quad (31)$$

Remark. We remark that for the particular linear case pertinent to Eq. (22), $\bar{\mathbf{J}}$ will be unaffected by $\bar{\phi}$. For further details we refer to Nilenius et al. [14] where the general non-linear case is considered.

5 Numerical example

The following numerical example serves to benchmark the proposed model. An SVE of with $L_{\square} = 2$ cm is considered with a volume fraction of aggregates of about 42 %, cf. Figure 6. We wish to determine the macroscale diffusivity tensor as a function of imposed macroscale strain in z -direction, i.e. we wish to determine the mapping

$$\bar{\varepsilon}_{zz} \mapsto \bar{\mathbf{D}}(\bar{\varepsilon}_{zz}). \quad (32)$$

We consider the linear problem $\mathbf{J} = -\mathbf{D} \cdot \nabla \phi$, where the local diffusivities are given in Eqs. (2), (3) and (12). As a result, the macroscale diffusivity tensor presented in Eq. (31) can be computed independently of $\bar{\phi}$ and $\bar{\mathbf{g}}$.

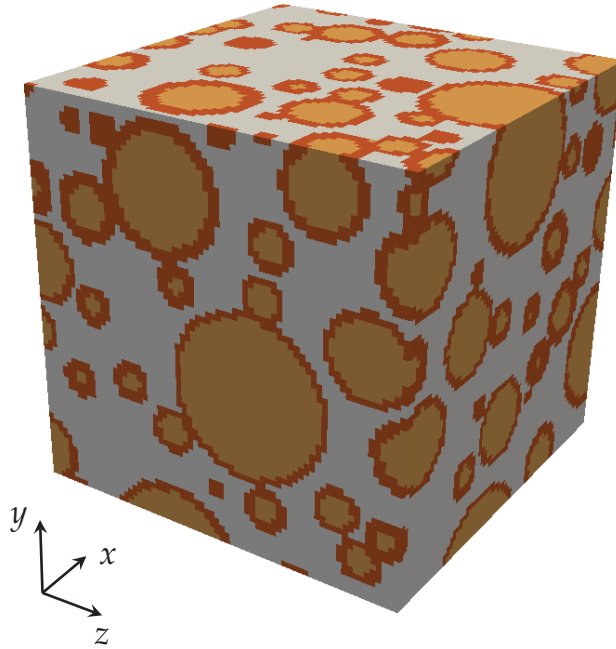


Figure 6: SVE used for the numerical example. The SVE has 343,000 elements and 1,073,733 DOF for the mechanical problem and 357,911 DOF for the diffusion problem.

5.1 Crack simulation

Model parameters pertaining to the mechanical problem are given in Table 1 below.

Table 1: Input parameters

Parameter	Description	Value
E_{cp}	Young's modulus of cement paste	35 GPa
E_a	Young's modulus of aggregates	70 GPa
E_{ITZ}	Young's modulus of ITZ	15.75 GPa
ν	Poisson's ratio	0.2
ϵ_{cr}	crack strain for both cement paste and ITZ	1×10^{-4}
A	model parameter in Eq. (15)	0.81
B	model parameter in Eq. (15)	10,450

The stress-strain relation for the SVE is shown in Figure 7, whereas Figure 8 shows the strain and crack evolution for the SVE. In the elastic regime—as seen in Figure 8a—the strain is concentrated in the ITZ attributed to the transversal isotropy modelling as described in Section 2.3.2. As the applied macroscale strain increases, the cracking strain, ε_{cr} , is eventually reached in the ITZ and cracking is then initiated. The crack propagation then follows the weak zone provided by the ITZ and is bridged over between aggregates through the cement paste which can be clearly seen in Figure 9.

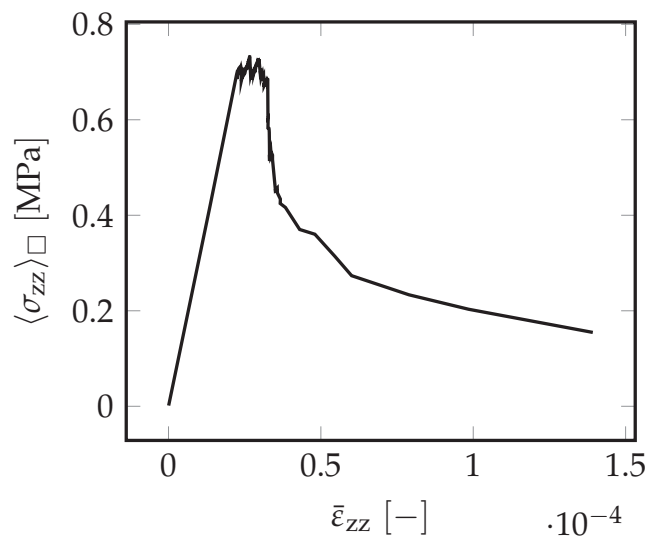
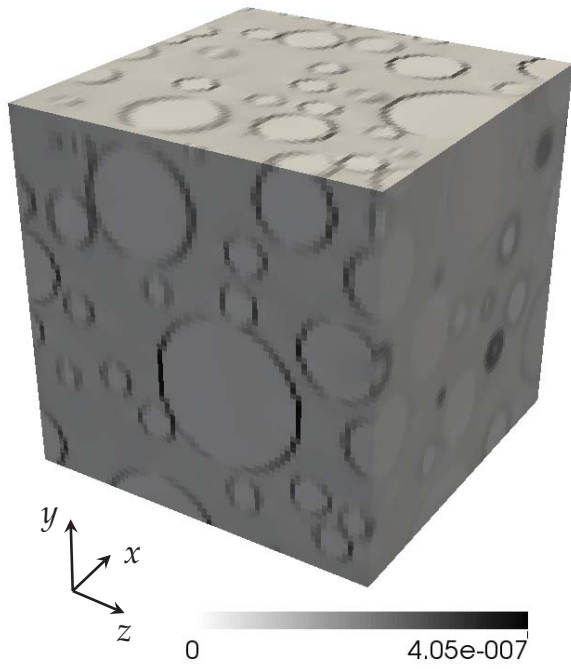
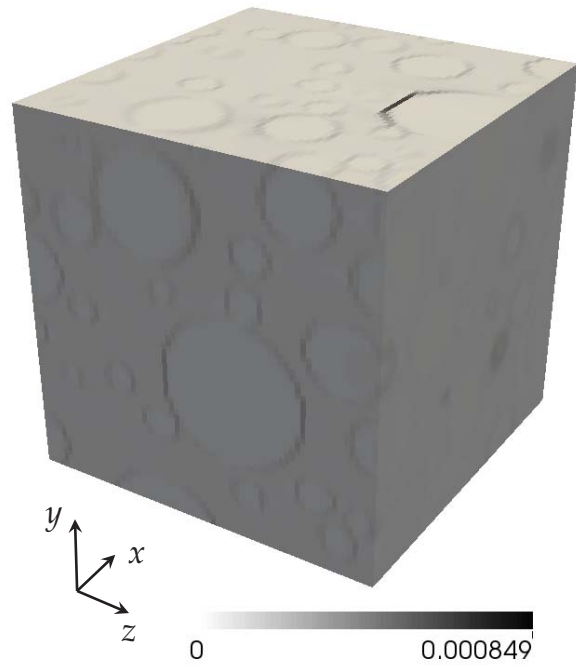


Figure 7: Homogenized stress versus applied macroscale strain in z -direction. The homogenized stress is computed by taking the volume average of σ_{zz} in the SVE.

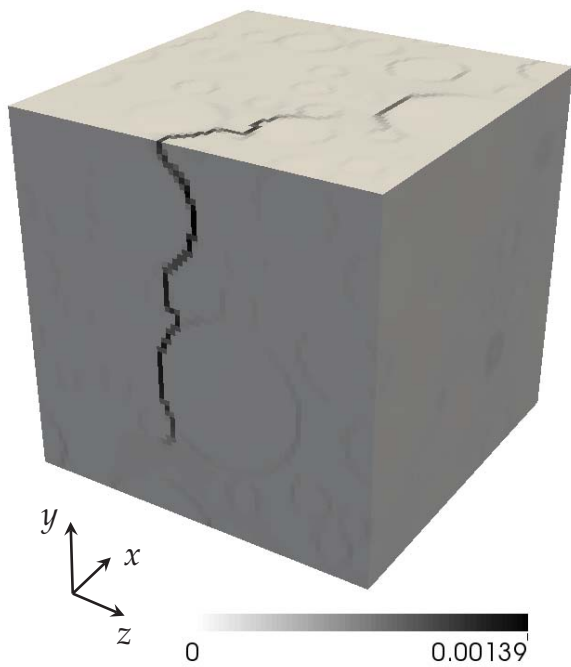
The macroscale stiffness of the SVE can be determined from Figure 7. Because of the ITZ, the slope in the elastic regime equals 30.7 GPa which is lower than both E_{cp} and E_a , cf. Table 1. Even though the aggregates are stiffer than the cement paste, the weak interface between the cement paste and aggregates decreases the macroscale stiffness and the net effect of aggregates is a reduction in stiffness of the SVE. This observation is in agreement with Mehta and Monteiro [13]. They claim that the ITZ is the reason why concrete is weaker than both cement paste and aggregates.



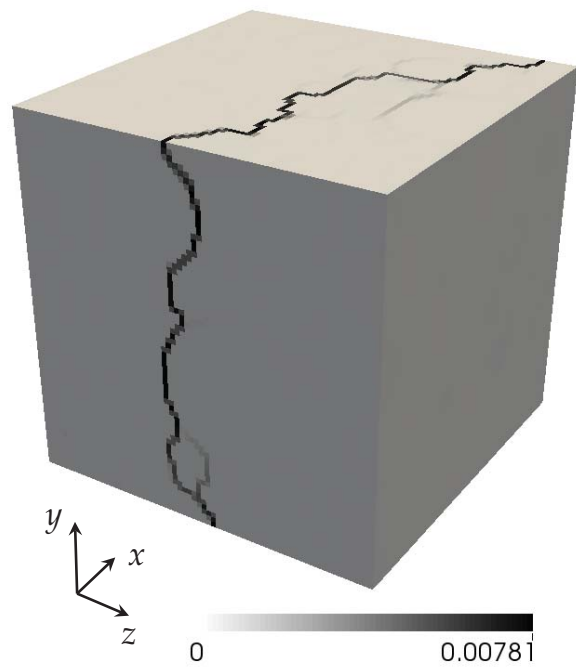
(a) $\bar{\epsilon}_{zz} = 5 \times 10^{-8}$.



(b) $\bar{\epsilon}_{zz} = 2.3877 \times 10^{-5}$.



(c) $\bar{\epsilon}_{zz} = 2.7580 \times 10^{-5}$.



(d) $\bar{\epsilon}_{zz} = 1.1021 \times 10^{-4}$.

Figure 8: Mesoscale strain evolution at different macroscale strain increments. Bar legends show maximal eigenstrain. Figure 8a is in the elastic regime while cracking has begun to develop in Figures 8b to 8d.

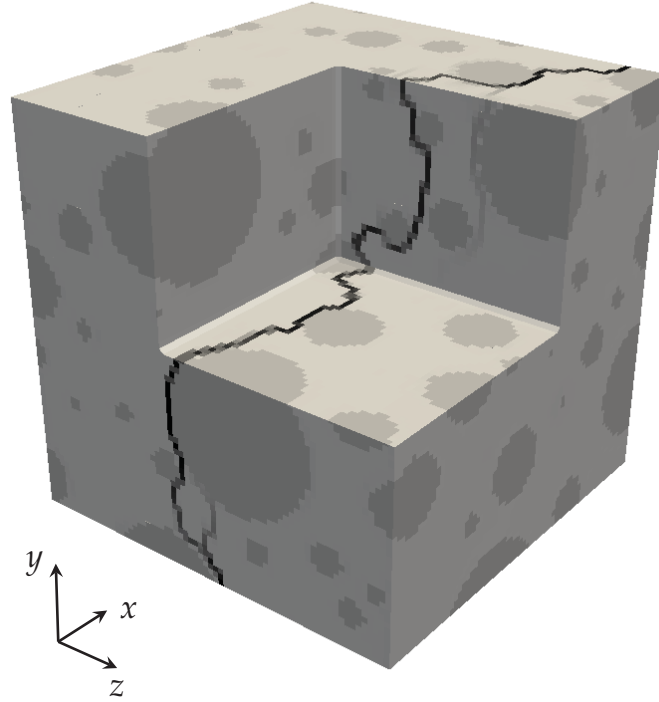


Figure 9: Cut out in the SVE showing how the crack path follows the ITZ. This is the same figure as Figure 8d but differently visualized.

5.2 Macroscale diffusivity

Once the mechanical problem has been solved, the macroscale diffusivity tensor can be computed from Eq. (31). Model parameters pertaining to the diffusion problem are given in Table 2. Two cases were studied: with and without diffusivity in the ITZ.

Table 2: *Input parameters*

Parameter	Description	Value
D_{cp}	diffusion coefficient of cement paste	1 cm/s^2
D_a	diffusion coefficient of aggregates	0 cm/s^2
\hat{D}_{ITZ}	diffusion coefficient of ITZ	$0.15 \times \hat{D}_{cp}$
D_{cr}	diffusion coefficient of crack	$50,000 \times D_{cp}$

Remark. Assuming the thickness of the ITZ to be $50 \mu\text{m}$ would correspond of a diffusivity in the ITZ equal to: $D_{ITZ} \times 50 \mu\text{m} = 0.15 \times \hat{D}_{cp} = 0.15 \times D_{cp} \times 1 \text{ cm} \Rightarrow D_{ITZ} = 30 \times D_{cp}$.

5.2.1 Without diffusivity in the ITZ

Figure 10 shows the component of the macroscale diffusivity tensor, $\bar{\mathbf{D}}$, as a function of applied macroscale strain for the SVE with diffusivity only in cement paste, i.e. the diffusivity in the ITZ was set equal to zero. While in the elastic regime, the diffusivity remains constant but once cracking is initiated at about $\hat{\epsilon}_{zz} = 3 \times 10^{-5}$, the diffusivity increases rapidly in value.

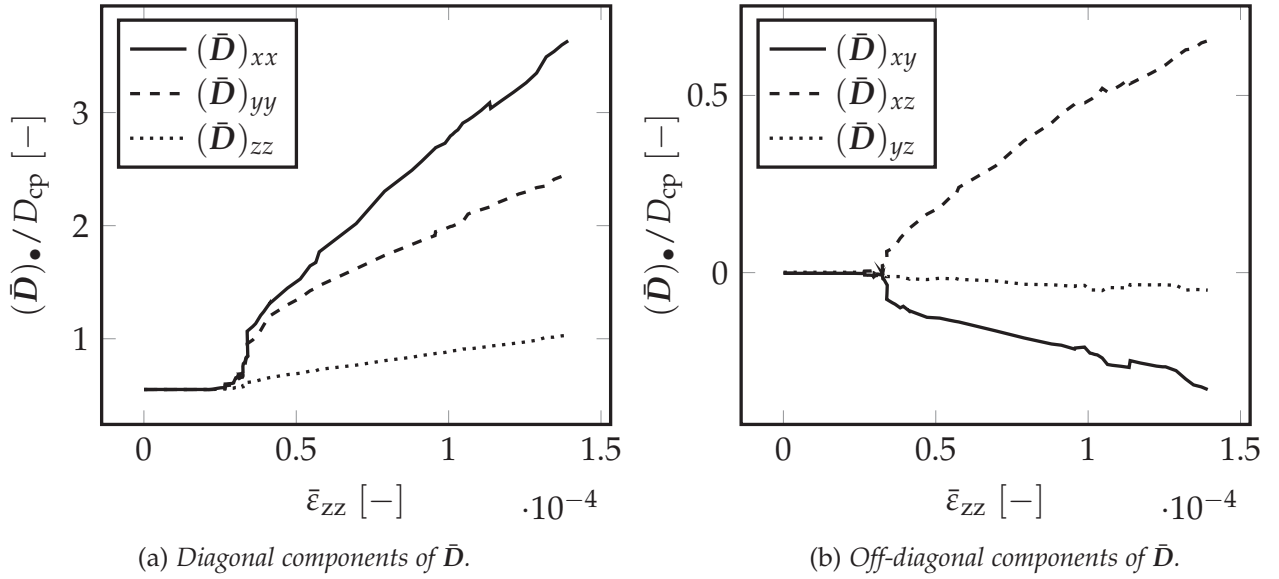


Figure 10: Components of the macroscale diffusivity tensor, $\bar{\mathbf{D}}$, as a function of macroscale strain. Numerical values are normalized with respect to D_{cp} . The diffusivity in the ITZ is zero in this example.

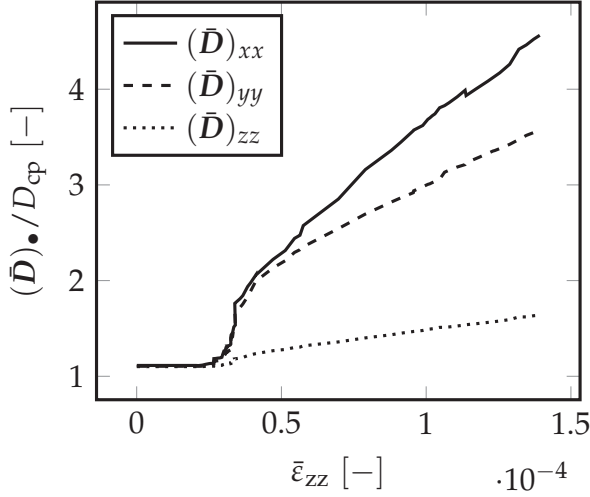
The anisotropy of the diffusivity tensor can be observed in Figure 10 since the diagonal components of $\bar{\mathbf{D}}$ do not increase in value by the same magnitude. Furthermore, the influence of material heterogeneities on the macroscale diffusivity is also apparent. If the SVE were homogeneous, a crack would develop in one plane perpendicular to the z -direction. For this SVE, however, the crack follows the surfaces of the aggregates and the global crack surface is rotated with respect to the z -direction as seen in Figure 8a. This explains why $(\bar{\mathbf{D}})_{xx}$ and $(\bar{\mathbf{D}})_{yy}$ differ in value in Figure 10a. For a homogeneous SVE, these two components would increase identically in value and $(\bar{\mathbf{D}})_{zz}$ would remain invariant to the applied strain.

Remark. For multiple SVE realizations, the mean difference between $(\bar{\mathbf{D}})_{xx}$ and $(\bar{\mathbf{D}})_{yy}$ is expected to tend to zero.

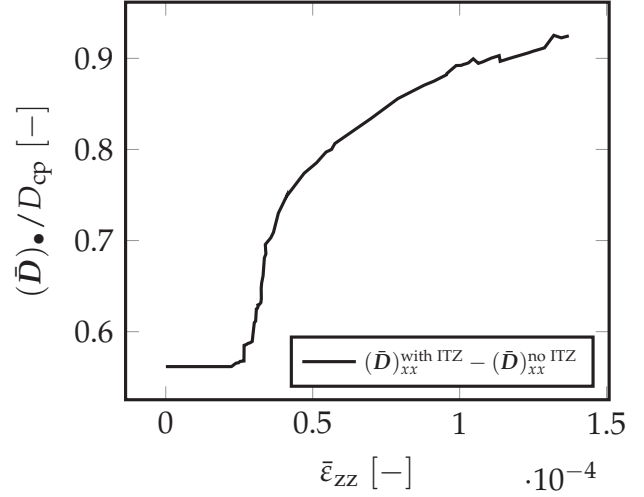
5.2.2 Influence on diffusivity of ITZ

The macroscale diffusivity tensor was also determined when a diffusivity in the ITZ was added, the results of which are shown in Figure 11. As seen in Figure 11b, by adding

diffusivity to the ITZ, the components of the homogenized macroscale diffusivity tensor $\bar{\mathbf{D}}$ are not increased by a constant as the crack develops. Instead, as the applied strain increases the ITZ yields a non-linear increase in diffusivity compared.



(a) Diagonal components of $\bar{\mathbf{D}}$ for $\hat{D}_{\text{ITZ}} = 0.15 \times \hat{D}_{\text{cp}}$.



(b) Difference in value between $(\bar{\mathbf{D}})_{xx}$ for $\hat{D}_{\text{ITZ}} = 0.15D_{\text{cp}}$ (i.e. with ITZ) and $\hat{D}_{\text{ITZ}} = 0$ (i.e. without ITZ).

Figure 11: Components of the macroscale diffusivity tensor, $\bar{\mathbf{D}}$, as a function of macroscale strain. Numerical values are normalized with respect to D_{cp} .

6 Conclusion and outlook

A model has been proposed to simulate crack-induced macroscale diffusivity of concrete by means of computational homogenization. The model is based on a three-dimensional (3D) Statistical Volume Element (SVE) of mesoscale concrete, in which the mesoscale constituents include the cement paste, aggregates and the Interfacial Transition Zone (ITZ).

The model provides a means to computationally correlate cracks to macroscale diffusivity in a novel fashion. The effects of the ITZ are also considered for both the mechanical problem of cracking as well as enhanced diffusivity.

The numerical results show that the macroscale diffusivity rapidly increases from its virgin value when cracking has been initiated. By the choice of constitutive model on the mesoscale level, the anisotropy of the macroscale diffusivity tensor of cracked concrete is captured. The crack propagation, in turn, could also be attributed to the material heterogeneities of the SVE in a realistic way. The results further show that the ITZ yields a non-linear increase in macroscale diffusivity when cracks are present in the SVE even though the diffusion coefficients of the ITZ and cracks were chosen to be constant.

Additionally, the proposed model is scalable in the sense that an SVE of arbitrary size—holding any realistic aggregate content—can be simulated as long as sufficient hardware resources required to solve the system of equations can be provided.

The model still needs further numerical investigation, in addition to calibration with experimental data. For instance, only a single SVE has been studied in this paper and the statistical scatter of the results has, therefore, not been quantified.

A natural extension of the model would be to consider the case where the macroscale diffusivity remains increased when the SVE is fully unstrained. Currently, cracks will fully close if the SVE is unstrained and the macroscale diffusivity will, consequently, in that case decrease to its virgin value.

Acknowledgments

This research was financially supported by The Swedish Research Council, which is gratefully acknowledged. The computations were performed on resources at the Chalmers Centre for Computational Science and Engineering (C³SE) provided by the Swedish National Infrastructure for Computing (SNIC).

References

- [1] A H Barbosa and A M P Carneiro. Micromechanical Modeling of the Elastic Modulus of the ITZ of Concrete. In W. Brameshuber, editor, *International RILEM Conference on Material Science*, volume II, pages 101–111. RILEM Publications SARL, 2010. ISBN 978-2-35158-108-7. D-9
- [2] E J Garboczi. Multiscale Analytical/Numerical Theory of the Diffusivity of Concrete. *Adv. Cem. Based Mater.*, 8(2):77–88, 1998. ISSN 10657355. doi: 10.1016/S1065-7355(98)00010-8. D-5
- [3] B Gérard and J Marchand. Influence of cracking on the diffusion properties of cement-based materials. *Cement and Concrete Research*, 30(1):37–43, January 2000. ISSN 00088846. doi: 10.1016/S0008-8846(99)00201-X. D-3
- [4] B. Gérard, D Breysse, A Ammouche, O. Houdusse, and O. Didry. Cracking and permeability of concrete under tension. *Materials and Structures*, 29(3):141–151, April 1996. ISSN 0025-5432. doi: 10.1007/BF02486159. D-3
- [5] P Grassl. A lattice approach to model flow in cracked concrete. *Cement and Concrete Comp.*, 31(7):454–460, 2009. ISSN 09589465. doi: 10.1016/j.cemconcomp.2009.05.001. D-3
- [6] M Hain and P Wriggers. Numerical homogenization of hardened cement paste. *Computational Mechanics*, 42(2):197–212, 2007. ISSN 0178-7675. doi: 10.1007/s00466-007-0211-9. D-5

-
- [7] M Hain and P Wriggers. Computational homogenization of micro-structural damage due to frost in hardened cement paste. *Finite. Elem. Anal. Des.*, 44(5): 233–244, 2008. ISSN 0168874X. doi: 10.1016/j.finel.2007.11.020. D-5
- [8] S Y Jang, B S Kim, and B H Oh. Effect of crack width on chloride diffusion coefficients of concrete by steady-state migration tests. *Cement and Concrete Research*, 41(1):9–19, January 2011. ISSN 00088846. doi: 10.1016/j.cemconres.2010.08.018. D-3
- [9] S Kim and R K A Al-rub. Meso-scale computational modeling of the plastic-damage response of cementitious composites. *Cement and Concrete Research*, 41(3):339–358, 2011. ISSN 0008-8846. doi: 10.1016/j.cemconres.2010.12.002. D-6
- [10] F Larsson, K Runesson, and F Su. Variationally consistent computational homogenization of transient heat flow. *Int. J. Numer. Meth. Eng.*, 81(13):1659–1686, 2009. ISSN 00295981. doi: 10.1002/nme.2747. D-12
- [11] L Liu, H Chen, W Sun, and G Ye. Microstructure-based modeling of the diffusivity of cement paste with micro-cracks. *Construction and Building Materials*, 38:1107–1116, January 2013. ISSN 09500618. doi: 10.1016/j.conbuildmat.2012.10.002. D-3
- [12] J Mazars. *Application de la mécanique de l'endommagement au comportement non linéaire et à la rupture du béton de structure*. PhD thesis, Université Paris VI, 1984. D-10
- [13] P K Mehta and P J M Monteiro. *Concrete: Microstructure, Properties and Materials*. McGraw-Hill Professional, 2006. ISBN 0071462899. doi: 10.1036/0071462899. D-15
- [14] F Nilenius, F Larsson, K Lundgren, and K Runesson. Computational homogenization of diffusion in three-phase mesoscale concrete. *Computation Mechanics*, 2014. D-4, D-13
- [15] A. U. Nilsen and P. J.M. Monteiro. Concrete: A three phase material. *Cement and Concrete Research*, 23(1):147–151, January 1993. doi: 10.1016/0008-8846(93)90145-Y. D-6
- [16] C Saouridis. *Identification et numérisation objectives des comportements adoucissants: Une approche multiéchelle de l'endommagement du béton*. PhD thesis, Université Paris VI, 1988. D-11
- [17] P Simeonov and S Ahmad. Effect of transition zone on the elastic behavior of cement-based composites. *Cement and Concrete Research*, 25(1):165–176, January 1995. ISSN 00088846. doi: 10.1016/0008-8846(94)00124-H. D-6
- [18] L Wang and T Ueda. Mesoscale modeling of water penetration into concrete by capillary absorption. *Ocean Engineering*, 38(4):519–528, 2011. ISSN 00298018. doi: 10.1016/j.oceaneng.2010.12.019. D-6
-